Alpha-synuclein oligomers stabilize pre-existing defects in supported bilayers and propagate membrane damage in a fractal-like pattern

Himanshu Chaudhary[†‡], *Aditya Iyer*[†§‡], *Vinod Subramaniam*[*†§‖] *and Mireille M.A.E. Claessens*[*†]

[†]Nanobiophysics Group, MESA[+] Institute for Nanotechnology and MIRA Institute for Biomedical Technology and Technical Medicine, Department of Science and Technology, University of Twente, 7500 AE, Enschede, The Netherlands

[§]Nanoscale Biophysics Group, FOM Institute AMOLF, Science Park 104, 1098 XG Amsterdam, The Netherlands

[‖]Vrije Universiteit Amsterdam, De Boelelaan 1105, 1081 HV Amsterdam, The Netherlands.

Corresponding Author

v.subramaniam@vu.nl

m.m.a.e.claessens@utwente.nl

[‡] These authors contributed equally to the work.

ABSTRACT

Phospholipid vesicles are commonly used to get insight into the mechanism by which oligomers of amyloidogenic proteins damage membranes. Oligomers of the protein α-synuclein (αS) are thought to create pores in phospholipid vesicles containing a high amount of anionic phospholipids but fail to damage vesicle membranes at lower surface charge densities. The current understanding of how αS oligomers damage membranes is thus incomplete. This incomplete understanding may, in part, result from the choice of model membrane systems. The use of free-standing membranes such as vesicles may interfere with unraveling some damage mechanisms, as the line tension of the edge of a membrane defect or pore ensures defect closure. Here we used supported lipid bilayers (SLBs) of POPC/POPS to study membrane damage caused by αS oligomers. Although αS oligomers were not able to initiate disruption of POPC/POPS vesicles or intact SLBs, oligomers did stabilize and enlarge pre-existing SLB defects. The increased exposure of lipid acyl chains at the edges of defects very likely facilitates membrane-oligomer interactions resulting in the growth of fractal domains devoid of lipids. Concomitant with the appearance of the fractal membrane damage patterns, lipids appear in solution, directly implicating αS oligomers in the observed lipid extraction. The growth of the membrane damage patterns is not limited by the binding of lipids to the oligomer. Analysis of the shape and growth of the lipid-free domains suggests the involvement of an oligomer-dependent diffusion limited extraction mechanism. The observed αS oligomer induced propagation of membrane defects offers new insights into mechanisms by which αS oligomers can contribute to the loss in membrane integrity.

INTRODUCTION

There is increasing evidence supporting the involvement of alpha-synuclein (αS) in not only the pathology[1] but also the etiology of Parkinson's disease (PD). It is believed that the aggregation of αS generates cytotoxic oligomeric species[2]. As for oligomers involved in several other protein aggregation diseases[3, 4, 5, 6], αS oligomers seem to possess the ability to disrupt lipid membranes and interfere with membrane-related processes leading to neuronal damage[3, 7] and cell death[2, 5, 8]. To obtain a better insight into oligomeric species and their toxicity mechanisms, *in vitro* prepared αS oligomers have been isolated and characterized using biophysical approaches[9, 10, 11, 12, 13], including single molecule fluorescence measurements[14, 15, 16]. Protocols for preparing αS oligomers vary considerably in the literature. Oligomer formation is induced by: including reactive aldehydes such as 4-oxo-2-nonenal (ONE) and 4-hydroxy-2-nonenal (HNE)[17, 18], dopamine[19], ethanol-$FeCl_3$ combinations[20], divalent cations[21], docosahexaenoic acid (DHA)[22], incubating at low-temperature[23], or simply elevating the αS concentrations[24]. Even when using one specific protocol, distinct species of oligomers with different structural properties have been observed[9]. The majority of these *in vitro* prepared oligomers are off-pathway to fibril formation; only the oligomers prepared in the presence of ONE have been reported to act as seeds for αS fibril growth *in vitro*[25]. These on-pathway ONE oligomers contain β-sheet structure and are toxic to neuronal cells[17, 18, 20, 22]. Interestingly, both on- and off-pathway αS oligomers prepared *in vitro* have been shown to permeabilize vesicles consisting of anionic phospholipids[3, 22, 26, 27, 28, 29, 30]. The interaction between the first 11 residues in the N-terminus of αS and the anionic membrane plays an important role in the permeabilization mechanism[27]. Although αS oligomers can disrupt the integrity of vesicles of composed of only anionic phospholipids, membrane permeabilization has not been observed in vesicles of several 1:1 mixtures of anionic and zwitterionic phospholipids including POPC/POPS and DOPE/DOPS[31]. This observation suggests that high surface charge densities

are required for disruptive oligomer-membrane interactions. Besides the above mentioned 1:1 mixtures, the integrity of membranes composed of more physiologically relevant lipid mixtures containing only ~ 15% anionic phospholipids also remains unaffected by αS oligomers. We have reported that αS oligomers cannot induce content leakage of vesicles composed of mixtures of brain PS:brain PE:cholesterol (2:5:3), mimicking the plasma membrane[28].

Most model studies on membrane disruption by amyloid oligomers are performed using phospholipid vesicles. However, *in vivo*, membranes are typically anchored to the cytoskeleton and extracellular matrix. Thus, free-standing membranes such as phospholipid vesicles, while convenient experimental systems, may not be suited to study all membrane damage mechanisms. Membrane rupture mechanisms involving non-trivial fractal rupture mechanics with crackling-noise avalanches, for example, cannot be observed in free-standing membranes[32]. To be able to judge if the inability of oligomers to induce membrane leakage from 1:1 mixtures of anionic and zwitterionic phospholipids results from the choice of the model membrane architecture, we investigated oligomer-induced damage in both free-standing and supported lipid bilayers (SLBs).

We show that both POPC/POPS GUVs and SLBs remain intact and do not show any sign of damage when incubated with αS oligomers. In contrast, in SLBs with pre-existing defects, oligomers were able to propagate membrane damage. Oligomers appeared to stabilize the defect edges and remove lipids from these edges resulting in fractal-like damage patterns. Concurrent with the membrane damage, lipid particles were observed to appear in solution. The fractal dimension D of the lipid-free defects was ~ 1.74, which is in agreement with an oligomer-dependent diffusion limited lipid extraction mechanism. Such mechanisms may become important during disruption of cell membranes in response to mechanical stress[33, 34, 35, 36], membrane remodeling processes[37, 38] or in aging cells where membrane recycling mechanisms are less efficient[39].

RESULTS

To enhance the interaction of oligomers with membranes, 1:1 mixtures of the zwitterionic lipid POPC and the anionic lipid POPS were used. We confirmed that monomeric and oligomeric αS does not interfere with the integrity of vesicles of this composition. We first monitored the effect of αS oligomers on the membrane integrity of POPC:POPS (1:1) GUVs. To be able to follow the vesicles in time, GUVs were anchored via biotinylated lipids to a streptavidin-coated surface. The GUVs were subsequently incubated with 2.5 μM of *in vitro* prepared, stable, well-characterized, αS oligomers[16] and imaged using confocal fluorescence microscopy. We observed that the GUVs remained spherical for at least 20 hours in both the absence and presence of αS oligomers (**Supporting Figure S1**). To check if αS oligomers did form (transient) pores in the membrane during this time period, we incubated GUVs with 10 μM of αS oligomers and additionally added the fluorescent dye calcein. In contrast to what has been observed for POPG GUVs[26], we observed no influx of calcein for up to 24 hours of incubation, the vesicle interior stayed devoid of calcein **(Supporting Figure S1)**. We this confirm that POPC:POPS (1:1) GUVs are resistant to αS oligomer-induced damage. We subsequently tested the effect of αS oligomers on the membrane integrity of POPC:POPS (1:1) SLBs under identical experimental conditions. Upon addition of 5 μM αS oligomers labeled with AlexaFluor488 (methods) to defect-free POPC/POPS SLBs prepared on bare glass substrates, we observed some sparse events of αS oligomer binding. This binding had however little impact on membrane integrity as neither membrane defects nor a decrease in fluorescence intensity from SLBs was observed (**Figure 1A-B**).

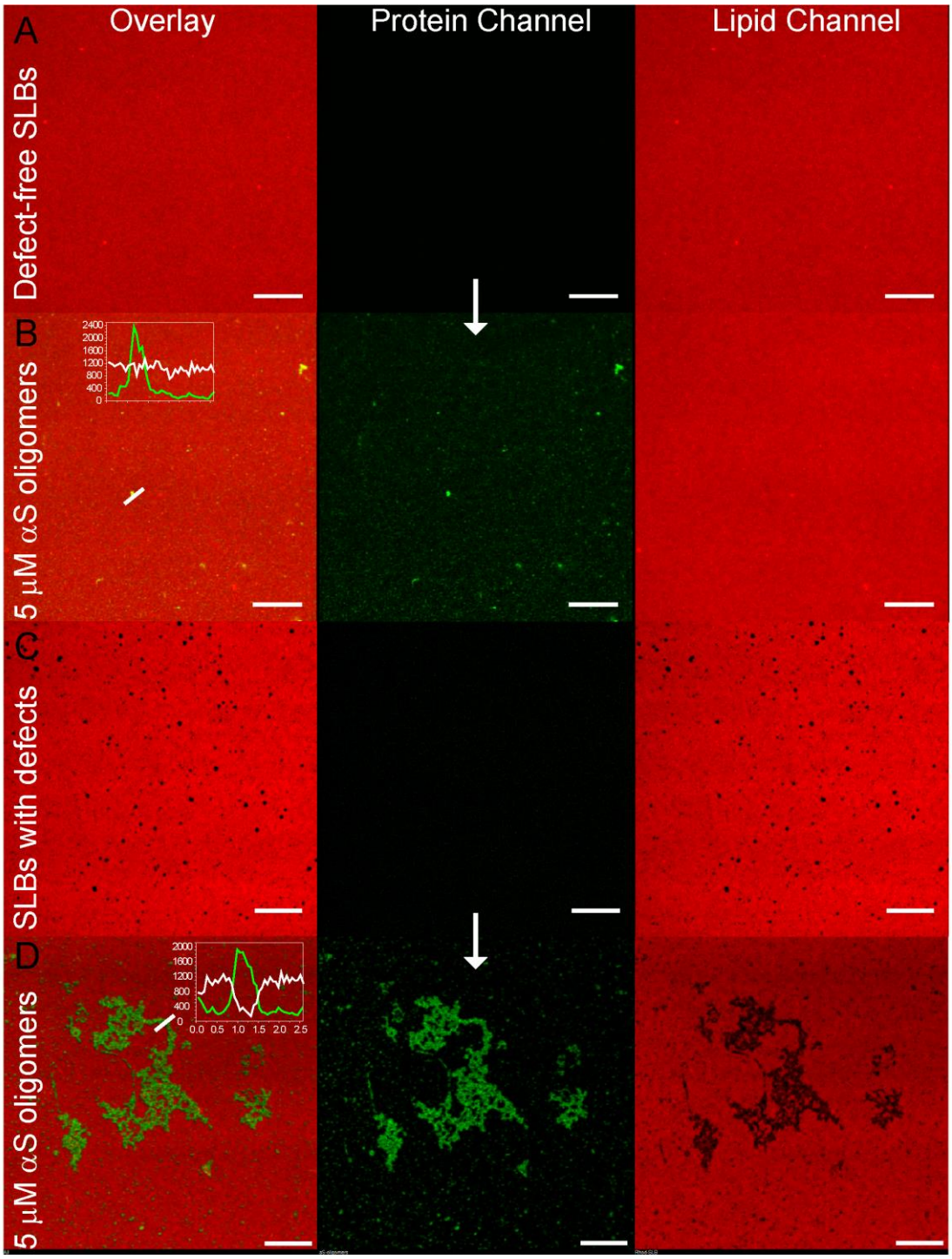

Figure 1: Effect of pre-existing defects in SLBs on αS oligomer interaction. Representative fluorescence images of defect free Rhod-PE labeled POPC/POPS SLB (lipid channel) after incubation of 5 µM AlexaFluor488 labeled αS oligomers (protein channel). Panel A and C depict images taken prior to incubation with αS oligomers. Six hours after addition of 5 µM αS oligomers (panel B), no visible membrane damage is seen in SLBs without preexisting defects while SLBs with pre-existing

defects contain characteristic damage patterns (panel D). All images were acquired at room temperature. The insets (panel B and D) show intensity profiles from the lipid (white) and protein channel (green). The lipid free defect areas contain labeled αS. The SLBs were buffered with 10 mM Tris-Cl, 100 mM NaCl at pH 7.4. Scale bar is 10 μm.

Interestingly, the addition of 5 μM αS oligomers to SLBs with pre-existing defects (**Figure 1C**) led to an increase in the defect area, a decrease in the fluorescence intensity in the lipid channel and to the appearance of fractal-like damage patterns that were filled with fluorescently labeled αS (**Figure 1D and Supporting Figure S2**). Six hours after oligomer addition, the relative increase in membrane defect area amounted ~500 % (**Figure 2A**). In control experiments, incubation with a comparable mass concentration of αS fibrils resulted in a ~140 % increase of lipid free area. In the absence of αS oligomers or fibrils, only a marginal increase in defect area of ~10% was observed (**control, Figure 2A)**. The increase in defect area in the presence of oligomers and fibrils did not simply result from the affinity of αS for the glass substrate since the addition of αS monomers led to a ~50% decrease in defect area (see also **Supplementary Figure S4A**). The observation that incubation with αS monomers results in a decrease in defect area is in line with previous observations and has been ascribed to insertion of αS in the lipid headgroup region resulting in lateral membrane expansion[40, 41]. Similar measurements with the protein BSA resulted in a negligibly small decrease in defect area of ~5%. The appearance of lipid-free regions is thus oligomer specific and possibly results from the extraction of lipids from the SLBs by oligomers. To confirm that the disappearance of lipids from the SLBs results from the presence of αS oligomers, we incubated a series of αS oligomer concentrations and buffer solution (control) with fluorescent BODIPY-PC lipid containing SLBs for 90 minutes. After 90 minutes, we monitored the increase in BODIPY-PC fluorescence in the solution above the SLBs. We observe a clear increase in fluorescence in this solution with increasing oligomer

concentration (**Figure 2B**). Oligomers indeed seem to extract lipids from POPC:POPS (1:1) SLBs when pre-existing defects are present.

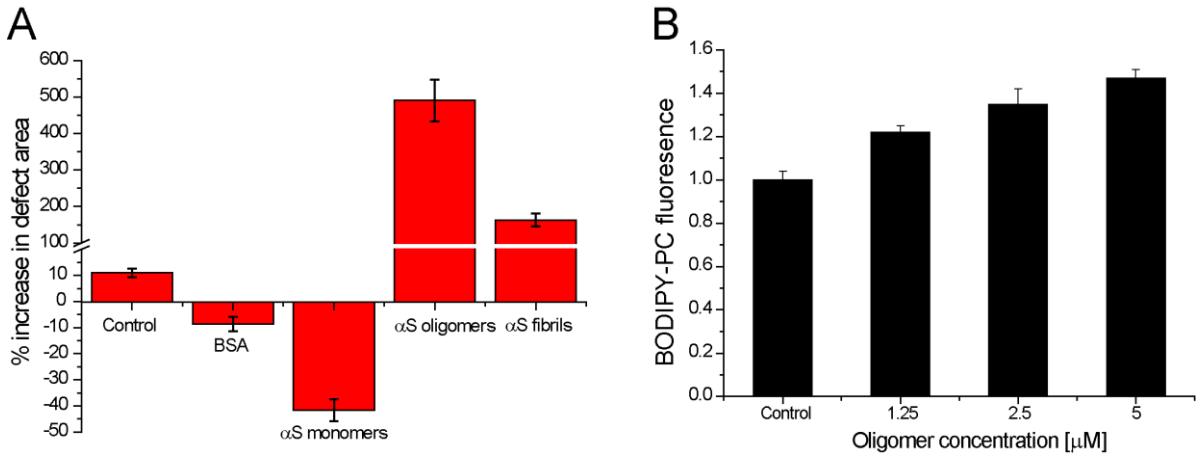

Figure 2: Lipid extraction from POPC/POPS SLBs by αS oligomers. A) Bar plots of relative increase in defect areas in SLBs (methods) upon incubation with 10 μM αS monomers, oligomers or fibrils for 6 hours. The effect of incubation with an identical mass concentration of bovine serum albumin (0.07 mg/ml) is shown as a control. The error bars indicate the s.d. of at least 5 independent regions in an SLB. B) A series of αS oligomer concentrations (0, 1.25, 2.5 and 5 μM) was incubated with 4 separate POPC:POPS (1:1) SLBs buffered at pH 7.4 in 10 mM Tris-Cl, 100 mM NaCl. Lipid extraction was followed by monitoring the BODIPY-PC fluorescence in the solution, above the bilayer after incubation for 90 minutes. The fluorescence was normalized to the control experiment in the absence of oligomer. The error bars indicate the SD of 3 independent measurements.

To exclude the possibility that the αS oligomer dependent appearance of fractal-like damage patterns in the SLBs result from an interaction of the oligomers with the glass substrate, other substrates were tested. Since grafting PEG to surfaces has been reported to reduce protein adsorption[42, 43], POPC:POPS (1:1) SLBs were prepared on PEG coated glass substrates. The addition of labeled αS oligomers to SLBs prepared on PEG surfaces resulted in membrane damage patterns similar to those observed on bare glass substrates. A time lapse of images of a growing SLB defect shows that the PEG coating indeed prevents protein adsorption; the defects

remain free of labelled protein (**Figure 3** compare to **Figure 1D**) Oligomers however still interact with and line up at membrane defect edges. The oligomer induced growth of existing SLB defects into damage patterns is comparable for SLBs prepared on glass and PEG coated glass substrates (**Supporting Figure S3**).

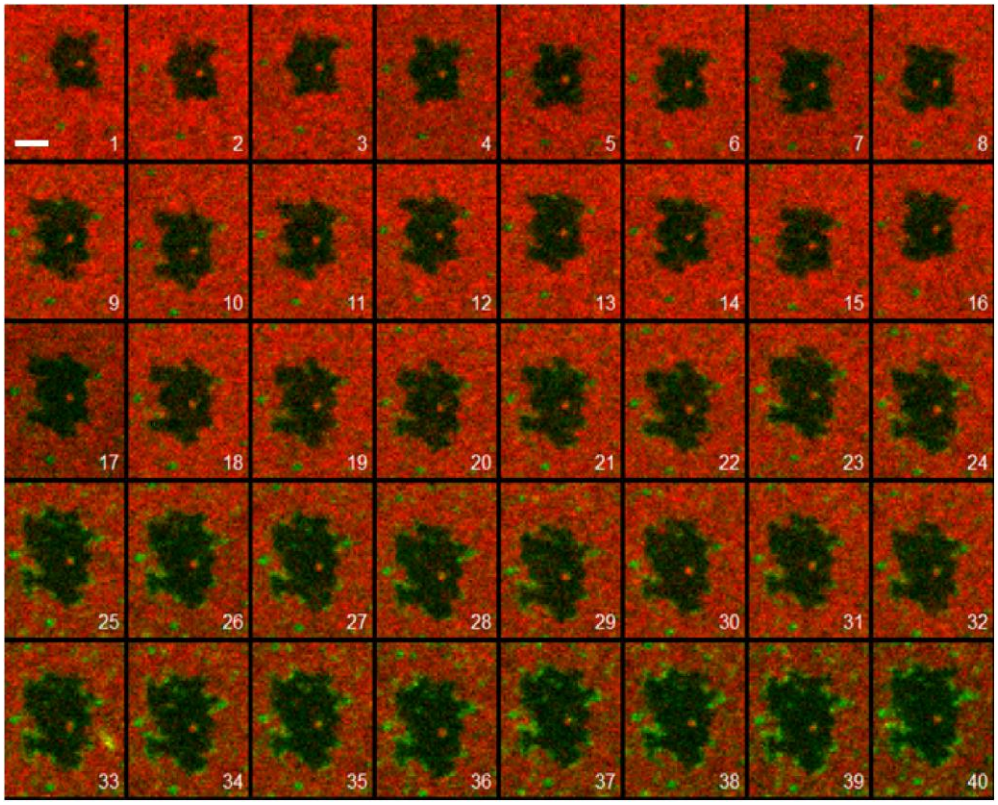

Figure 3: Confocal time-lapse of images showing the evolution of damage patterns in POPC:POPS (1:1) SLBs on a PEG coated glass surfaces. The addition of 5 μM AlexaFluor488 labeled αS oligomers (green) to Rhod-PE containing POPC/POPS SLBs with pre-existing defects prepared on a PEG coated surface leads to their recruitment along edges of damage patterns. The frames are numbered (1-40) and were acquired at 10 minute intervals. The SLBs were buffered at pH 7.4 with 10 mM Tris-Cl, 100 mM NaCl at room temperature. Scale bar is 2 μm.

To visualize the membrane damage with a higher lateral and height resolution, we further investigated the damage patterns using atomic force microscopy (AFM). We prepared POPC:POPS (1:1) SLBs with defects on freshly cleaved mica surface. A height profile along

one of these defects indicated that the SLBs were approximately 5 nm thick (**Supplementary Figure S4B**), which agrees well with the thickness of a single bilayer. Subsequently 2.5 μM αS oligomers were incubated with the defect containing SLBs (**Figure 4**). Within 10 minutes, αS oligomers were seen to start filling up the defects, and after ~50 minutes, the defects were completely filled (**Figure 4E**). As observed in the fluorescence microcopy experiments, we consistently observed a gradual loss of lipids from the SLBs. This loss of lipids seems to spread in a pattern that appears to emanate from αS oligomer-filled defect edges only. It is therefore likely that these edges act as damage nucleation sites. One of the nucleation sites is indicated by a white arrow in **Figure 4F.**

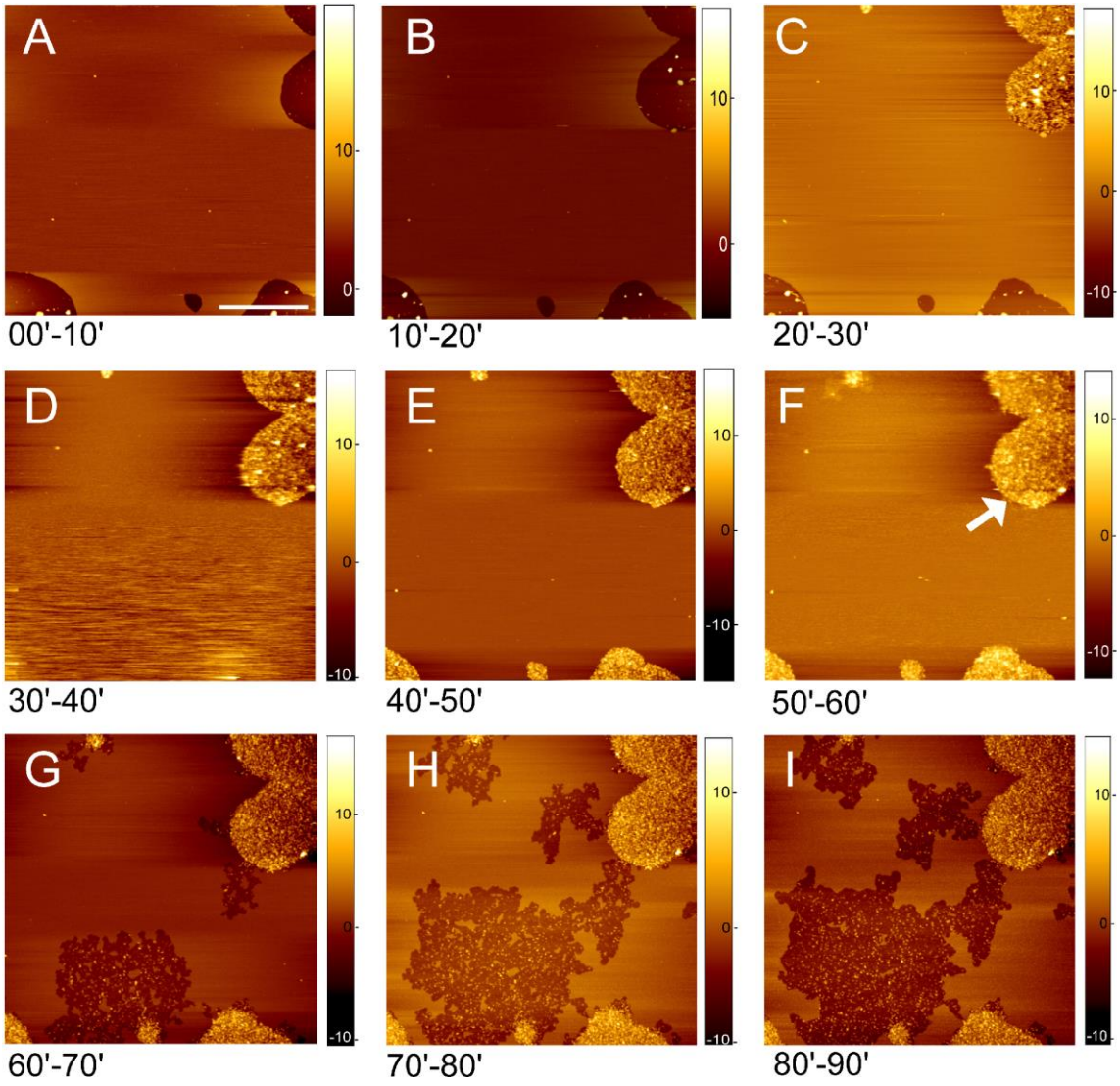

Figure 4: Time-lapse AFM images of membrane defect propagation by αS oligomers. Panels A-I show AFM images of the POPC/POPS (1:1) SLBs in the presence of 2.5 μM αS oligomers. The images where obtained at 10 minute intervals. Initially oligomers were recruited to the defects in the SLBs. The recruitment of oligomers in defects starts from 0', no additional membrane damage is observed for up to 50 minutes (A-E). The white arrow indicates initiation of destructive extraction of lipids from preexisting defects. The growth of the damage patterns becomes more apparent in (F-I). Scale bar is 2 μm.

From the edge of the αS oligomer-filled defect, the membrane damage propagates outwards, causing the membrane to break up into a fractal like pattern, which results in the appearance of several membrane islands (**Figure 5**). Independent AFM experiments showed that membrane

damage consistently initiates from oligomer-filled defects resulting in similar SLB damage patterns (**Supporting Figure S5**). No membrane damage was observed to arise from defect-free regions. Moreover, as observed in the confocal fluorescence microscopy measurements, we hardly ever observe oligomers on the lipid bilayer in AFM measurements. This may result from the low binding affinity of αS oligomers for POPC/POPS membranes and is in agreement with earlier GUV experiments[24].

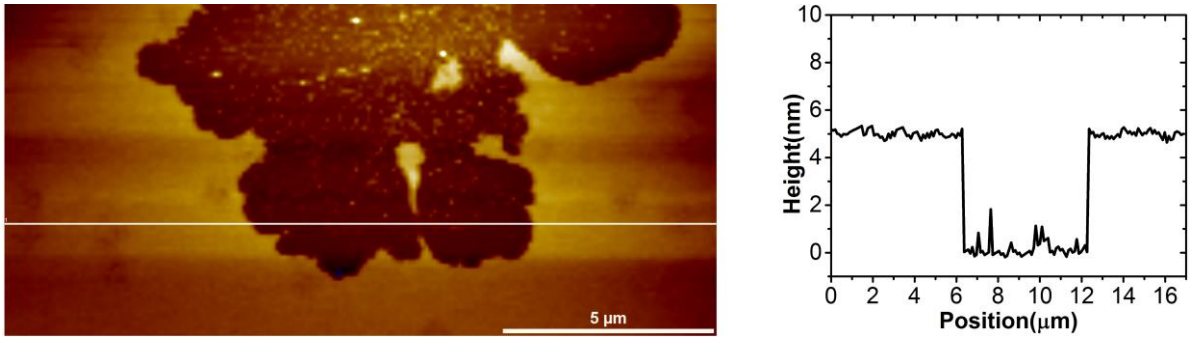

Figure 5: AFM image of a fractal damage pattern in a POPC/POPS SLB after addition of 2.5 µM αS oligomers (left panel). The panel on the right depicts the height profile, corresponding to the white line in the left panel, confirming loss of the complete bilayer. Scale bar is 5 µm.

A closer look at the damaged SLBs shows small structures (white regions in **Figure 5**), which may be oligomers or oligomer-lipid aggregates. An AFM height profile indicates that these structures are roughly twice the size of SLBs (~6 nm), a bit smaller than the diameter reported for stable in vitro prepared αS oligomers[13]. The non-circular shape of the oligomer induced defects and the binding of oligomers to the edges of the defect borders indicates that oligomers somehow stabilize the damage patterns (**Supplementary Figure S6**). The oligomer induced damage patterns resemble fractals (**Figure 6A**). To establish their fractal nature, we employed fractal dimension analysis (methods) using the box-counting method (**Figure 6B**). Irrespective of the underlying SLB substrate or the imaging method, the average fractal dimension *D* was ~ 1.74 ± 0.04 (**Figure 6C**). This value for *D* is typically found for diffusion-limited processes[44, 45, 46].

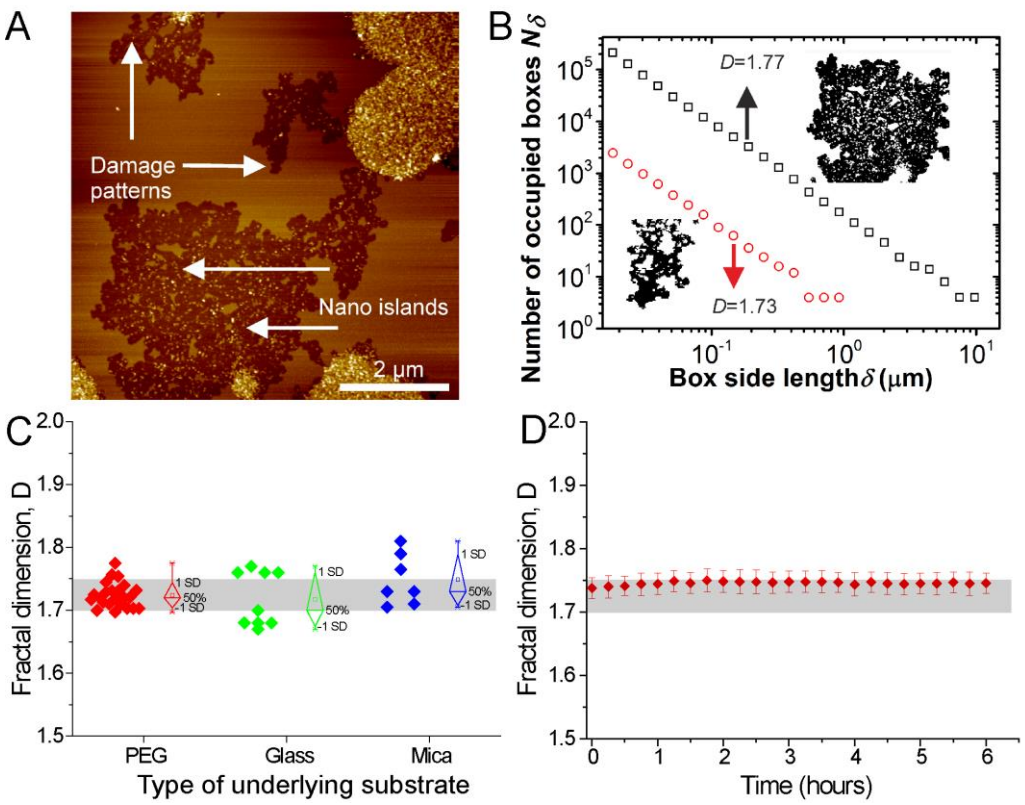

Figure 6: Fractal analysis of membrane damage patterns. A) Representative AFM image depicting fractal like damage patterns. B) Results of fractal analysis using box-counting method for two AFM images. C) Comparison of fractal dimensions of membrane damage patterns obtained for SLBs prepared on different supports. Every point in panel A represents a fractal dimension from an individual fractal. D) Evolution of fractal dimensions during defect expansion over time on PEG-supported SLBs in presence of 5 µM αS oligomers. The error bars indicate standard deviations from at least 10 independent fractals. The gray bars depict the range of D from 1.7 to 1.75.

The fractal dimension *D* of the membrane damage patterns did not depend on the substrate underlying the SLBs. This suggests that the mechanism by which the damage patterns formed is not primarily determined by interactions between the substrate-membrane and/or substrate-αS oligomers. When the oligomer induced damage patterns in SLBs grew in size with time, the fractal dimensions did not change significantly (**Figure 6D)**. The latter observation is in agreement with the scale-invariant nature of fractals.

Discussion

The understanding of how oligomer-membrane interactions are related to cytotoxicity in PD is inadequate. To obtain a mechanistic understanding of cytotoxic events that directly result from oligomer-membrane interactions, numerous studies with model membranes have been performed. In these *in vitro* studies, mainly free-standing membranes such as vesicles have been used. It has been shown that oligomers have high affinity for highly negatively charged membranes, and impair the integrity of negatively charged phospholipid vesicles. Upon interaction of oligomers with GUVs composed of the anionic phospholipid POPG, the membrane becomes leaky, but the overall vesicle morphology remains intact[26]. As the percentage of negatively charged lipids in the membrane is decreased, the surface charge density decreases and damage caused by oligomers diminishes[31].

The phospholipid phosphatidylserine is one of the most common anionic phospholipids in eukaryotic membranes. It is especially prevalent in the inner leaflet of the plasma membrane[47]. However, no significant oligomer-induced leakage of dyes from LUVs and GUVs mimicking the inner plasma membrane (Brain PS/ brain PC/ cholesterol) has been observed. Even at higher ratios, such as POPC/POPS 1:1, oligomers do not cause damage in GUVs. It would be interesting to see if increasing membrane affinity using organic solvents or ferric ions results in pore formation/membrane thinning[48, 49]. Although monomeric αS has been reported to bind POPC/POPS membranes, the affinity of αS for these membranes seems considerably lower than the affinity for POPC/POPG containing membranes[24]. The low affinity of αS monomers for membranes is also observed for oligomers; no co-localization of isolated *in vitro* produced oligomers with POPC/POPS vesicles could be observed[24]. Due to their low affinity for POPC/POPS membranes, oligomers do not generate pores or cause membrane thinning in such vesicles. The lack of oligomer induced damage in membranes with a high PS content suggests

that PS rich membranes, such as the plasma membrane, are the not initiation sites for membrane damage. However, this phenomenon may be biased by the choice of the membrane model system.

In cells, plasma membranes are typically supported by other cellular structures like the cytoskeleton and the extra-cellular matrix. In our experiments on supported POPC/POPS membranes, we report a non-trivial mechanism of oligomer-induced membrane damage. Whereas the addition of oligomers to GUVs or intact SLBs did not results in membrane damage, oligomers were able to enlarge preexisting SLB defects. The addition of αS oligomers to SLBs with preexisting defects resulted in the extraction of lipids from the SLBs and an increase in the damage area and contour length. The increase in lipid fluorescence in the solution with increasing αS oligomer concentration shows that extraction indeed results from interactions with αS oligomers. As reported for GUVs, we did not observe binding of the oligomers to the membrane surface, instead oligomers colocalized with the SLB defect contour. The high tension and curvature of the membrane defects probably allows membrane edges to act as nucleation sites for spreading damage (**Figure 7**). Such defects, where high curvature causes exposure of hydrophobic areas, are not present or are very short lived in GUVs and LUVs and this damage mechanism is therefore absent in these systems. Destructive lipid membrane extraction is initiated from the contours of preexisting rounded SLB defects and propagated in an irregularly shaped fractal like pattern. The irregular shapes of the αS oligomer induced damage patterns do not agree with the expected high mobility of lipids in the SLBs and rounded shapes of defects observed in the absence of protein (**Supplementary Figure S6**). Reorganization of the membrane is not simply prevented by surface adsorbed protein; fractal like damage patterns are also observed in SLBs on PEG coated surfaces. The shape of the damage patterns and the observed alignment of oligomers at the edges of the defects indicates that the binding of αS oligomers somehow stabilizes the entire contour of the membrane defect. The stabilization of

membrane defects by αS oligomers and membrane remodeling by αS monomers observed in our study emanate from different driving forces. The binding of αS monomers to lipid membranes does not require defects. It is well known to be driven by both electrostatic and hydrophobic interactions[27, 41, 50, 51, 52]. Monomer binding involves the insertion of an amphipathic helix which is stabilized by interactions of the aligned positively charged lysine's in this helix with the negatively charged lipids. Although monomers may also stabilize defect edges, the insertion of monomers into the lipid bilayer decreases the size of the pores in the SLBs and thus the exposed edge length. Oligomers on the other hand expand defects and thereby increase the exposed defect edge length.

The damage footprint resulting from oligomer-induced lipid extraction showed fractal like characteristics. Further analysis of this membrane damage pattern resulted in an average fractal dimension D of ~1.74 ± 0.04 irrespective of underlying substrate used. These values are consistent with the proposed diffusion limited lipid extraction by oligomers as opposed to a reaction limited process where D would be larger than 2[53, 54, 55]. In a reaction limited lipid extraction process the extraction process itself would be rate limiting. This is apparently not the case, instead the diffusion of oligomers to a reactive membrane site is limiting the extraction process. Once they reach this defect site, lipid extraction is fast. After lipid extraction oligomers/lipid particles most likely disappear and therefore no gradient of oligomers is observed along the edge of the damage pattern in AFM experiments (**Figure 6**).

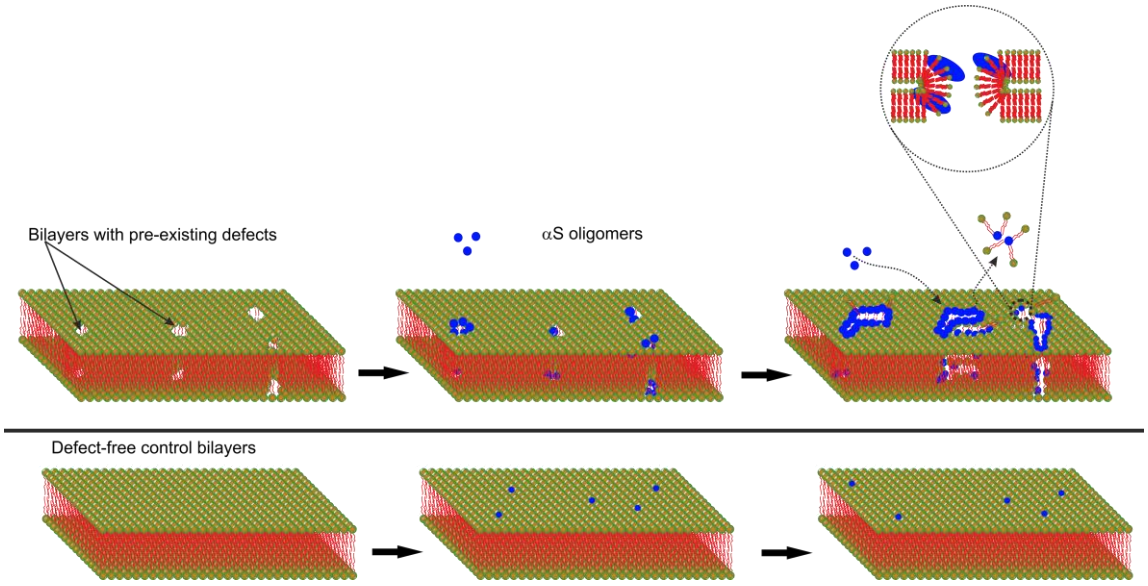

Figure 7: Model for diffusion limited lipid extraction by αS oligomers.

Our results indicate that in spite of the low affinity of isolated oligomers for lipid bilayers with physiologically relevant surface charge densities, the presence of oligomers may become problematic. Transient membrane defects possible appear during vesicle fusion events[37,36] and as a result of mechanical stress[33, 34, 35, 36]. Also, aging of cells typically leads to a decrease in membrane lipid dynamics and an increase in the replenishment time of membrane lipids[39]. As a result, once membranes of aged cells become damaged, the chances to recruit oligomers to the damage site increase. A recent report suggests that mitochondrial membranes might be a potential target for αS oligomers due to their intrinsic mechanical instability and packing defects[52]. Compared to reaction limited extraction mechanisms, the contour of the newly created SLB edges enormously increases upon lipid extraction. Such large edged contours stabilized entirely by αS oligomers may become difficult to close and will have numerous opportunities to interact with other cellular components. It is therefore tempting to speculate that the mechanism of oligomer-induced lipid extraction from pre-existing damage sites observed *in vitro* may also be relevant *in vivo*. Transient defects in aged cellular membranes could recruit αS oligomers which potentially stabilize or even enlarge these defects resulting in

loss of cytoplasmic constituents. The observed oligomer dependent lipid extraction mechanism may therefore have serious consequences for cells.

CONCLUSION

It is generally accepted that αS oligomers damage membranes by pore formation or membrane thinning, but in model studies isolated oligomeric αS only affects the integrity of vesicles with a high percentage of anionic lipids. In this report, we show that although oligomeric αS cannot initiate the disruption of 1:1 POPC/POPS bilayers, these species can stabilize and subsequently expand pre-existing membrane defects by a lipid extraction mechanism that is diffusion limited. Destructive phospholipid extraction from membranes by oligomers could be another route to membrane damage.

EXPERIMENTAL

Materials. Stock solutions of 1-palmitoyl-2-oleoyl-sn-glycero-3-phosphocholine (POPC), 1-palmitoyl-2-oleoyl-sn-glycero-3-phospho-L-serine (POPS) were purchased from Avanti Polar Lipids (Birmingham, AL) and used without further purification. Alexa Fluor 647 C2 maleimide and β-BODIPY® FL C5-HPC (2-(4,4-Difluoro-5,7-Dimethyl-4-Bora-3a,4a-Diaza-s-Indacene-3-Pentanoyl)-1-Hexadecanoyl-sn-Glycero-3-Phosphocholine (BODIPY-PC) was purchased from Invitrogen (Carlsbad, CA). Ethylenediaminetetraacetic acid (EDTA) was purchased from Sigma Chemicals (St. Louis, MO). Sodium chloride (NaCl), sodium hydroxide (NaOH), and Tris(hydroxymethyl)aminomethane (Tris) were purchased from Merck (Germany). Bottomless, 6-channel Sticky-Slide VI$^{0.4}$ chambers were purchased from ibidi® (Germany) and were directly annealed to cleaned glass cover-slips before use.

Expression and purification. αS was expressed in *Escherichia coli* strain BL21 (DE3) using the pT7-7 expression plasmid and purified in the presence of 1 mM DTT as previously reported[56].

Preparation of αS oligomers. αS oligomers were prepared as described previously[28]. For preparation of labeled oligomers for fluorescence microscopy and spectroscopy experiments, 10% of the monomers used for the preparation of oligomers were labeled with AlexaFluor 488 dye. The concentration of oligomers was determined by measuring the absorption at 276 nm using a Shimadzu UV-visible spectrophotometer. The protein labeling efficiency was estimated to be >90% from the absorption spectrum by measuring protein absorbance at 280 nm (A_{280}) using the molar extinction coefficient at 280 nm (i.e. ε_{280} = 5120 cm^{-1} M^{-1}) and including the correction factor for AlexaFluor 488 absorbance (ε_{495} = 73000 cm^{-1} M^{-1}) at 280 nm. Oligomers were stored at 4 °C and used within 2-3 days of preparation.

Preparation of giant unilamellar vesicles (GUVs). Lipid mixtures were prepared from a 10 mg/ml stock solution of POPC and POPS in chloroform. To allow visualization of the vesicles using fluorescence microscopy, 0.05% of Lissamine Rhodamine PE (Avanti Polar Lipids, Birmingham, AL) was included in the mixtures. Additionally, the phospholipid mixtures contained 0.01% 18:1 Biotinyl PE lipids that were introduced to facilitate immobilization of vesicles on streptavidin-coated glass slides. GUVs were prepared by the electro-formation method using a platinum (Pt) wire electrode with a diameter of 0.762 mm in a 1 ml plastic cuvette. The lipids suspended in chloroform were deposited on the wire drop by drop, and were dried using a nitrogen stream. After drying of the lipids the electrodes were transferred to a cuvette filled with 700 µl of electroswelling buffer (100 mM NaCl, 100 mM sucrose and 10 mM Tris-Cl, pH 7.4) and connected to a frequency generator (PCGUI 1000 Velleman). The electroswelling was done at 500 Hz, and during detachment of vesicles the frequency was

gradually decreased from 500-50Hz as reported elsewhere[57]. For all experimental conditions the electroswelling was done at room temperature using the same frequency generator settings.

Preparation of coated glass slides. To anchor GUVs to the surface, cover-slips were incubated with streptavidin (100 μg/ml) in phosphate buffered saline (PBS) for 30 minutes. Thereafter, the slides were rinsed with 10 mM Tris-Cl, 100 mM glucose, 100 mM NaCl buffered at pH 7.4 to remove unbound streptavidin and ensure osmotic balance with the GUV containing solution. The biotinylated GUVs were subsequently incubated on these cover-slips for 10-15 minutes in buffer solution and used for imaging and further experiments.

Confocal microscopy and image analysis. Immobilized GUVs were visualized using a Zeiss CLSM 510 confocal microscope with a 63X Plan-Apochromat 1.4 NA oil immersion objective. For confocal imaging of SLBs, a Nikon A1 confocal microscope equipped with a perfect focus system (PFS) was used. Images were acquired using a 100X oil immersion, 1.49 NA objective. Lissamine Rhodamine-DOPE (Rh-DOPE) was excited at 543 nm using a Helium Neon laser and calcein/Alexa488 labeled αS oligomers were excited with the 488 nm Argon laser line. The fluorescent signals from Rh-DOPE and calcein/Alexa488 labeled αS oligomers were acquired in sequential mode to minimize crosstalk. For the quantification of defect areas, raw images of the Rh-DOPE labeled SLBs were first converted to binary scale. Subsequently the total pixel area corresponding to area of each defect was determined using the Nikon NIS Elements *ObjectCount* plugin. Laser intensity and gain settings were kept constant for all experiments.

Substrate pretreatment for SLB preparation. Glass cover-slips were washed in 2% Hellmanex (VWR International, Chicago, IL) at 80 °C for 60 minutes, rinsed extensively with deionized water and then dried with a stream of nitrogen. The cover-slips were etched for 8 minutes in a solution of 3:1 (v/v) concentrated sulfuric acid (H_2SO_4) and 30% hydrogen peroxide (H_2O_2). The slides were stored in deionized water, and were used within 3 days. For

the preparation of PEG coated glass substrates, a previously reported protocol was followed[58]. The mobility of the SLBs on the PEG coated glass was measured using the fluorescence recovery after photobleaching (FRAP) technique. The lipids in the SLBs prepared on PEG coated glass substrates had ~2.5 fold higher diffusion coefficient as compared to those on bare glass substrates.

Preparation of large unilamellar vesicles (LUVs) and supported lipid bilayers (SLBs). Lipid stock solutions of POPC and POPS in chloroform were mixed in 1:1 molar ratios, dried under a stream of nitrogen, and placed under vacuum for 1 hour. After drying, the lipid films were rehydrated in 100 mM NaCl solution to a final concentration of 500 μM and vortexed vigorously. Thereafter, they were freeze-thawed for at least six times resulting in a clear suspension of unilamellar vesicles. Large unilamellar vesicles were prepared by extruding the freeze-thawed solution 21 times through a 100 nm polycarbonate membrane. The vesicles were stored at 4 °C and used within 3 days. SLBs were formed by vesicle fusion on freshly cleaved mica or pretreated glass slides. For preparation of SLBs with defects, the extruded vesicles in 100 mM NaCl were mixed with 400 mM NaCl solution at a 1:1 ratio in a custom-built chamber to induce surface adhesion and vesicle fusion. After 20 minutes of incubation, the chamber was rinsed with 10 mM Tris-Cl, 100 mM NaCl, pH 7.4 buffer. For preparation of defect-free SLBs, the extruded vesicles in 100 mM NaCl were mixed with 1 M NaCl in a 1:1 ratio and thereafter the procedure described above was followed. For lipid extraction experiments SLBs were prepared from POPC/POPS vesicles doped with 0.5 % of BODIPY-PC.

Atomic force microscopy (AFM) experiments. Imaging of SLBs on mica was done using tapping-mode AFM in ambient conditions on a Bioscope Catalyst instrument (Bruker Santa Barbara CA, USA). The experiments were performed under ambient conditions in buffer solution while circumventing fluid evaporation. Proteins in 10 mM Tris-Cl, 100 mM NaCl, pH 7.4 buffer appropriate amounts were added to SLBs using a Hamilton® syringe. Tapping mode

AFM imaging in fluid was done using MSCT nonconductive silicon nitride probes (MSCT tip F, K=0.6 N/m) mounted on a CAT-FCH probe holder (Bruker Camarillo, CA, USA). Imaging was performed at low force settings to avoid disruptive interactions with the sample.

Lipid extraction assay. SLBs composed of POPC/POPS (1:1) were formed by vesicle fusion inside a 6-channel sticky-Slide $VI^{0.4}$ chamber (Ibidi®, Germany) by simply annealing these chambers to the treated cover-slips. Thereafter, the buffer solution above the SLBs was collected (while keeping the SLBs hydrated) and BODIPY-PC fluorescence or the supernatant was measured in a TECAN InfinitePro M200 plate reader. Appropriate concentrations of αS oligomers were then flushed into the chamber and incubated for 60 minutes. After 60 minutes, the buffer solution was again collected and the BODIPY-PC fluorescence in the supernatant was quantified.

Fractal Analysis. For fractal analysis, the AFM and fluorescence microscopy images were first converted into binary bitmap images by using ImageJ. The fractal dimension of the damage patterns in the thus obtained binary images was determined using the box-counting method[45] in BENOIT™ software v.1.3.1. Briefly, the box counting method calculates the fractal dimension of a given image by superimposing it with a grid consisting of boxes of size δ. By counting the number of boxes N required to regenerate the whole area of interest and subsequently iterating this procedure on the same image with varying δ, $N(\delta)$ is obtained:

$$\ln(N(\delta)) = -D * ln\,(\delta)$$

Where the proportionality constant D is the fractal dimension. The software and the box-counting method was validated against fractals of known dimensionality, e.g., Sierpinski triangle (D = 1.585) and a black square (D = 2) before applying them to the membrane damage patterns.

ASSOCIATED INFORMATION

Supporting Information: Six additional figures and detailed description of

AUTHOR INFORMATION

Corresponding Author

v.subramaniam@vu.nl, m.m.a.e.claessens@utwente.nl

Author Contribution

HC and AI contributed equally to the work. HC, AI, MMAEC, and VS conceived the experiments. HC and AI designed and performed the experiments. All authors reviewed and analyzed the results and approved the final version of the manuscript.

Notes

The authors declare no competing financial interests.

ACKNOWLEDGMENTS

The authors thank Nathalie Schilderink and Kirsten A. van Leijenhorst-Groener for assistance with αS expression, purification, and labeling. The authors acknowledge Prof. Bela Mulder, Dr. Cristina Martinez Torres from FOM Institute AMOLF, The Netherlands and Somya Mani from National Centre for Biological Sciences, India for critical reading of the manuscript. This work was supported by the FOM program titled “A Single Molecule View on Protein Aggregation” and by a VIDI grant (700.59.423) from the Netherlands Organization for Scientific Research (NWO) to MMAEC.

REFERENCES

1. Spillantini, M. G.; Schmidt, M. L.; Lee, V. M.; Trojanowski, J. Q.; Jakes, R.; Goedert, M. Alpha-synuclein in Lewy bodies. Nature 1997, 388 (6645), 839-840.
2. Drews, A. Investigating How A beta and alpha Synuclein Oligomers Initially Damage Neuronal Cells. Biophys. J. 2014, 106 (2), 548a-548a.
3. Winner, B.; Jappelli, R.; Maji, S. K.; Desplats, P. A.; Boyer, L.; Aigner, S.; Hetzer, C.; Loher, T.; Vilar, M.; Campionic, S.; Tzitzilonis, C.; Soragni, A.; Jessberger, S.; Mira, H.; Consiglio, A.; Pham, E.; Masliah, E.; Gage, F. H.; Riek, R. In vivo demonstration that alpha-synuclein oligomers are toxic. P Natl Acad Sci USA 2011, 108 (10), 4194-4199.
4. Serra-Vidal, B.; Pujadas, L.; Rossi, D.; Soriano, E.; Madurga, S.; Carulla, N. Hydrogen/deuterium exchange-protected oligomers populated during Abeta fibril formation correlate with neuronal cell death. ACS Chem Biol 2014, 9 (11), 2678-85.
5. Kalia, L. V.; Kalia, S. K.; McLean, P. J.; Lozano, A. M.; Lang, A. E. alpha-Synuclein oligomers and clinical implications for Parkinson disease. Ann. Neurol. 2013, 73 (2), 155-69.
6. Stefani, M. Structural features and cytotoxicity of amyloid oligomers: Implications in Alzheimer's disease and other diseases with amyloid deposits. Prog. Neurobiol. 2012, 99 (3), 226-245.
7. Lorenzen, N.; Otzen, D. E. Oligomers of alpha-synuclein: picking the culprit in the line-up. Amyloids in Health and Disease 2014, 56, 137-148.
8. Andreasen, M.; Lorenzen, N.; Otzen, D. Interactions between misfolded protein oligomers and membranes: A central topic in neurodegenerative diseases? Biochimica et biophysica acta 2015, 1848 (9), 1897-907.
9. Paslawski, W.; Mysling, S.; Thomsen, K.; Jorgensen, T. J.; Otzen, D. E. Co-existence of two different alpha-synuclein oligomers with different core structures determined by hydrogen/deuterium exchange mass spectrometry. Angewandte Chemie, International Edition in English 2014, 53 (29), 7560-3.
10. Lorenzen, N.; Nielsen, S. B.; Buell, A. K.; Kaspersen, J. D.; Arosio, P.; Vad, B. S.; Paslawski, W.; Christiansen, G.; Valnickova-Hansen, Z.; Andreasen, M.; Enghild, J. J.; Pedersen, J. S.; Dobson, C. M.; Knowles, T. P.; Otzen, D. E. The Role of Stable alpha-Synuclein Oligomers in the Molecular Events Underlying Amyloid Formation. Journal of the American Chemical Society 2014.
11. Kim, H. Y.; Cho, M. K.; Kumar, A.; Maier, E.; Siebenhaar, C.; Becker, S.; Fernandez, C. O.; Lashuel, H. A.; Benz, R.; Lange, A.; Zweckstetter, M. Structural properties of pore-forming oligomers of alpha-synuclein. Journal of the American Chemical Society 2009, 131 (47), 17482-9.
12. Chen, S. W.; Drakulic, S.; Deas, E.; Ouberai, M.; Aprile, F. A.; Arranz, R.; Ness, S.; Roodveldt, C.; Guilliams, T.; De-Genst, E. J.; Klenerman, D.; Wood, N. W.; Knowles, T. P. J.; Alfonso, C.; Rivas, G.; Abramov, A. Y.; Valpuesta, J. M.; Dobson, C. M.; Cremades, N. Structural characterization of toxic oligomers that are kinetically trapped during α-synuclein fibril formation. Proceedings of the National Academy of Sciences 2015, 112 (16), E1994-E2003.
13. Stefanovic, A. N.; Lindhoud, S.; Semerdzhiev, S. A.; Claessens, M. M.; Subramaniam, V. Oligomers of Parkinson's Disease-Related alpha-Synuclein Mutants Have Similar Structures but Distinctive Membrane Permeabilization Properties. Biochemistry 2015, 54 (20), 3142-50.

14. Tosatto, L.; Horrocks, M. H.; Nunilo, C.; Guilliams, T.; Dalla Serra, M.; Klenerman, D. Single Molecule FRET Characterization of Oligomers from Alpha-Synuclein Early Onset Parkinson's Disease Mutants. Biophys. J. 2014, 106 (2), 268a-268a.
15. Horrocks, M. H.; Lee, S. F.; Gandhi, S.; Iljina, M.; Tosatto, L.; Dobson, C. M.; Klenerman, D. Single-Molecule Characterisation of Alpha-Synuclein Oligomers. Biophys. J. 2014, 106 (2), 267a-267a.
16. Zijlstra, N.; Blum, C.; Segers-Nolten, I. M.; Claessens, M. M.; Subramaniam, V. Molecular composition of sub-stoichiometrically labeled alpha-synuclein oligomers determined by single-molecule photobleaching. Angewandte Chemie, International Edition in English 2012, 51 (35), 8821-4.
17. Nasstrom, T.; Fagerqvist, T.; Barbu, M.; Karlsson, M.; Nikolajeff, F.; Kasrayan, A.; Ekberg, M.; Lannfelt, L.; Ingelsson, M.; Bergstrom, J. The lipid peroxidation products 4-oxo-2-nonenal and 4-hydroxy-2-nonenal promote the formation of alpha-synuclein oligomers with distinct biochemical, morphological, and functional properties. Free Radical Biol. Med. 2011, 50 (3), 428-437.
18. Bae, E. J.; Ho, D. H.; Park, E.; Jung, J. W.; Cho, K.; Hong, J. H.; Lee, H. J.; Kim, K. P.; Lee, S. J. Lipid Peroxidation Product 4-Hydroxy-2-Nonenal Promotes Seeding-Capable Oligomer Formation and Cell-to-Cell Transfer of alpha-Synuclein. Antioxidants & Redox Signaling 2013, 18 (7), 770-783.
19. Cappai, R.; Leck, S. L.; Tew, D. J.; Williamson, N. A.; Smith, D. P.; Galatis, D.; Sharples, R. A.; Curtain, C. C.; Ali, F. E.; Cherny, R. A.; Culvenor, J. G.; Bottomley, S. P.; Masters, C. L.; Barnham, K. J.; Hill, A. F. Dopamine promotes alpha-synuclein aggregation into SDS-resistant soluble oligomers via a distinct folding pathway. FASEB J. 2005, 19 (8), 1377-+.
20. Danzer, K. M.; Haasen, D.; Karow, A. R.; Moussaud, S.; Habeck, M.; Giese, A.; Kretzschmar, H.; Hengerer, B.; Kostka, M. Different species of alpha-synuclein oligomers induce calcium influx and seeding. J. Neurosci. 2007, 27 (34), 9220-9232.
21. Lowe, R.; Pountney, D. L.; Jensen, P. H.; Gai, W. P.; Voelcker, N. H. Calcium(II) selectively induces alpha-synuclein annular oligomers via interaction with the C-terminal domain. Protein Sci 2004, 13 (12), 3245-3252.
22. Fecchio, C.; De Franceschi, G.; Relini, A.; Greggio, E.; Dalla Serra, M.; Bubacco, L.; Polverino de Laureto, P. alpha-Synuclein Oligomers Induced by Docosahexaenoic Acid Affect Membrane Integrity. PLoS One 2013, 8 (11), e82732.
23. Lashuel, H. A.; Petre, B. M.; Wall, J.; Simon, M.; Nowak, R. J.; Walz, T.; Lansbury, P. T. alpha-synuclein, especially the Parkinson's disease-associated mutants, forms pore-like annular and tubular protofibrils. J. Mol. Biol. 2002, 322 (5), 1089-1102.
24. van Rooijen, B. D.; Claessens, M. M.; Subramaniam, V. Membrane binding of oligomeric alpha-synuclein depends on bilayer charge and packing. FEBS letters 2008, 582 (27), 3788-92.
25. Fagerqvist, T.; Nasstrom, T.; Ihse, E.; Lindstrom, V.; Sahlin, C.; Tucker, S. M.; Kasaryan, A.; Karlsson, M.; Nikolajeff, F.; Schell, H.; Outeiro, T. F.; Kahle, P. J.; Lannfelt, L.; Ingelsson, M.; Bergstrom, J. Off-pathway alpha-synuclein oligomers seem to alter alpha-synuclein turnover in a cell model but lack seeding capability in vivo. Amyloid 2013, 20 (4), 233-44.
26. van Rooijen, B. D.; Claessens, M. M.; Subramaniam, V. Membrane Permeabilization by Oligomeric alpha-Synuclein: In Search of the Mechanism. PLoS One 2010, 5 (12), e14292.
27. Lorenzen, N.; Lemminger, L.; Pedersen, J. N.; Nielsen, S. B.; Otzen, D. E. The N-terminus of alpha-synuclein is essential for both monomeric and oligomeric interactions with membranes. FEBS letters 2014, 588 (3), 497-502.

28. Stefanovic, A. N.; Stockl, M. T.; Claessens, M. M.; Subramaniam, V. alpha-Synuclein oligomers distinctively permeabilize complex model membranes. The FEBS journal 2014, 281 (12), 2838-50.
29. Camilleri, A.; Zarb, C.; Caruana, M.; Ostermeier, U.; Ghio, S.; Hogen, T.; Schmidt, F.; Giese, A.; Vassallo, N. Mitochondrial membrane permeabilisation by amyloid aggregates and protection by polyphenols. Biochim Biophys Acta 2013, 1828 (11), 2532-43.
30. Caruana, M.; Neuner, J.; Hogen, T.; Schmidt, F.; Kamp, F.; Scerri, C.; Giese, A.; Vassallo, N. Polyphenolic compounds are novel protective agents against lipid membrane damage by alpha-synuclein aggregates in vitro. Biochim Biophys Acta 2012, 1818 (11), 2502-10.
31. van Rooijen, B. D.; Claessens, M. M.; Subramaniam, V. Lipid bilayer disruption by oligomeric alpha-synuclein depends on bilayer charge and accessibility of the hydrophobic core. Biochim. Biophys. Acta 2009, 1788 (6), 1271-8.
32. Gozen, I.; Dommersnes, P.; Czolkos, I.; Jesorka, A.; Lobovkina, T.; Orwar, O. Fractal avalanche ruptures in biological membranes. Nature materials 2010, 9 (11), 908-12.
33. Clarke, M. S. F.; Caldwell, R. W.; Chiao, H.; Miyake, K.; Mcneil, P. L. Contraction-Induced Cell Wounding and Release of Fibroblast Growth-Factor in Heart. Circul. Res. 1995, 76 (6), 927-934.
34. Mcneil, P. L.; Khakee, R. Disruptions of Muscle-Fiber Plasma-Membranes - Role in Exercise-Induced Damage. Am J Pathol 1992, 140 (5), 1097-1109.
35. McNeil, P. L.; Steinhardt, R. A. Loss, restoration, and maintenance of plasma membrane integrity. J. Cell Biol. 1997, 137 (1), 1-4.
36. McNeil, P. L.; Terasaki, M. Coping with the inevitable: how cells repair a torn surface membrane. Nat. Cell Biol. 2001, 3 (5), E124-E129.
37. Steinhardt, R. A.; Bi, G. Q.; Alderton, J. M. Cell-Membrane Resealing by a Vesicular Mechanism Similar to Neurotransmitter Release. Science 1994, 263 (5145), 390-393.
38. Terasaki, M.; Miyake, K.; McNeil, P. L. Large plasma membrane disruptions are rapidly resealed by Ca2+-dependent vesicle-vesicle fusion events. J. Cell Biol. 1997, 139 (1), 63-74.
39. Levi, M.; Wilson, P.; Nguyen, S.; Iorio, E.; Sapora, O.; Parasassi, T. In K562 and HL60 cells membrane ageing during cell growth is associated with changes in cholesterol concentration. Mechanisms of Ageing and Development 1997, 97 (2), 109-119.
40. Ouberai, M. M.; Wang, J.; Swann, M. J.; Galvagnion, C.; Guilliams, T.; Dobson, C. M.; Welland, M. E. alpha-Synuclein senses lipid packing defects and induces lateral expansion of lipids leading to membrane remodeling. The Journal of biological chemistry 2013, 288 (29), 20883-20895.
41. Braun, A. R.; Lacy, M. M.; Ducas, V. C.; Rhoades, E.; Sachs, J. N. alpha-Synuclein-induced membrane remodeling is driven by binding affinity, partition depth, and interleaflet order asymmetry. J Am Chem Soc 2014, 136 (28), 9962-72.
42. Gölander, C.-G.; Herron, J. N.; Lim, K.; Claesson, P.; Stenius, P.; Andrade, J. D. Properties of Immobilized PEG Films and the Interaction with Proteins. In Poly(Ethylene Glycol) Chemistry: Biotechnical and Biomedical Applications, Harris, J. M., Ed.; Springer US: Boston, MA, 1992, pp 221-245.
43. Alcantar, N. A.; Aydil, E. S.; Israelachvili, J. N. Polyethylene glycol-coated biocompatible surfaces. Journal of Biomedical Materials Research 2000, 51 (3), 343-351.
44. Witten, T. A.; Sander, L. M. Diffusion-Limited Aggregation, a Kinetic Critical Phenomenon. Phys. Rev. Lett. 1981, 47 (19), 1400-1403.
45. Dewey, T. G. Fractals in molecular biophysics; Oxford University Press: Oxford, 1997.

46. Moran-Mirabal, J. M.; Aubrecht, D. M.; Craighead, H. G. Phase separation and fractal domain formation in Phospholipid/Diacetylene-Supported lipid bilayers. Langmuir 2007, 23 (21), 10661-10671.
47. van Meer, G.; Voelker, D. R.; Feigenson, G. W. Membrane lipids: where they are and how they behave. Nature reviews. Molecular cell biology 2008, 9 (2), 112-24.
48. Hogen, T.; Levin, J.; Schmidt, F.; Caruana, M.; Vassallo, N.; Kretzschmar, H.; Botzel, K.; Kamp, F.; Giese, A. Two different binding modes of alpha-synuclein to lipid vesicles depending on its aggregation state. Biophys J 2012, 102 (7), 1646-55.
49. Kostka, M.; Hogen, T.; Danzer, K. M.; Levin, J.; Habeck, M.; Wirth, A.; Wagner, R.; Glabe, C. G.; Finger, S.; Heinzelmann, U.; Garidel, P.; Duan, W.; Ross, C. A.; Kretzschmar, H.; Giese, A. Single particle characterization of iron-induced pore-forming alpha-synuclein oligomers. J Biol Chem 2008, 283 (16), 10992-1003.
50. Iyer, A.; Roeters, S. J.; Schilderink, N.; Hommersom, B.; Heeren, R. M.; Woutersen, S.; Claessens, M. M.; Subramaniam, V. The Impact of N-terminal Acetylation of Alpha Synuclein on Phospholipid Membrane Binding and Fibril Structure. The Journal of biological chemistry 2016.
51. Garten, M.; Prevost, C.; Cadart, C.; Gautier, R.; Bousset, L.; Melki, R.; Bassereau, P.; Vanni, S. Methyl-branched lipids promote the membrane adsorption of alpha-synuclein by enhancing shallow lipid-packing defects. Physical chemistry chemical physics : PCCP 2015, 17 (24), 15589-97.
52. Ghio, S.; Kamp, F.; Cauchi, R.; Giese, A.; Vassallo, N. Interaction of alpha-synuclein with biomembranes in Parkinson's disease--role of cardiolipin. Prog Lipid Res 2016, 61, 73-82.
53. Martin, J. E. Slow aggregation of colloidal silica. Physical review. A, General physics 1987, 36 (7), 3415-3426.
54. Martin, J. E.; Wilcoxon, J. P.; Schaefer, D.; Odinek, J. Fast aggregation of colloidal silica. Physical review. A 1990, 41 (8), 4379-4391.
55. Lin, M. Y.; Lindsay, H. M.; Weitz, D. A.; Klein, R.; Ball, R. C.; Meakin, P. Universal Diffusion-Limited Colloid Aggregation. J Phys-Condens Mat 1990, 2 (13), 3093-3113.
56. van Raaij, M. E.; Segers-Nolten, I. M.; Subramaniam, V. Quantitative morphological analysis reveals ultrastructural diversity of amyloid fibrils from alpha-synuclein mutants. Biophys J 2006, 91 (11), L96-8.
57. Pott, T.; Bouvrais, H.; Meleard, P. Giant unilamellar vesicle formation under physiologically relevant conditions. Chem. Phys. Lipids 2008, 154 (2), 115-9.
58. Jimenez, J.; Heim, A. J., 2nd; Matthews, W. G.; Alcantar, N. Construction and characterization of soft-supported lipid bilayer membranes for biosensors application. Conference proceedings : ... Annual International Conference of the IEEE Engineering in Medicine and Biology Society. IEEE Engineering in Medicine and Biology Society. Annual Conference 2006, 1, 4119-22.

TOC graphic

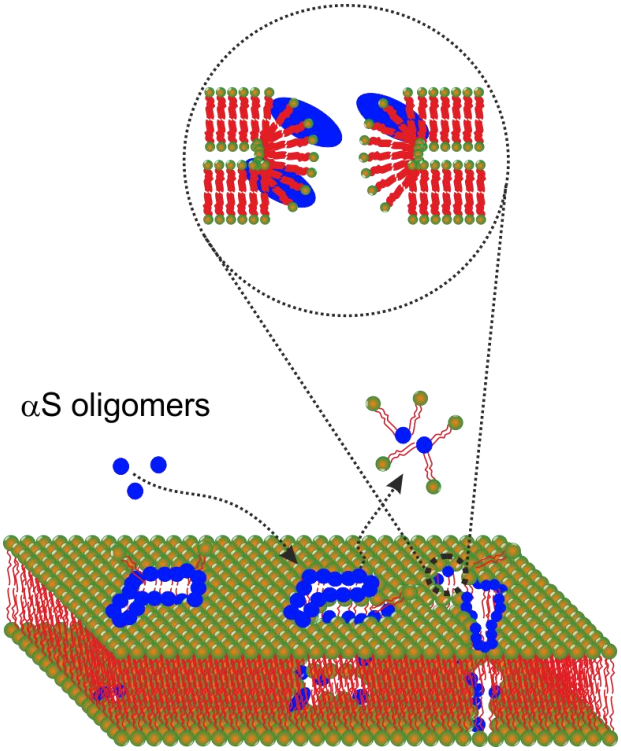

Supporting Information

Alpha-synuclein oligomers stabilize pre-existing defects in supported bilayers and propagate membrane damage in a fractal-like pattern

Himanshu Chaudhary[†], *Aditya Iyer*[†§], *Vinod Subramaniam*[*†§‖] *and Mireille M.A.E. Claessens*[*†]

[†]Nanobiophysics Group, MESA[+] Institute for Nanotechnology and MIRA Institute for Biomedical Technology and Technical Medicine, Department of Science and Technology, University of Twente, 7500 AE, Enschede, The Netherlands

[§]Nanoscale Biophysics Group, FOM Institute AMOLF, Science Park 104, 1098 XG Amsterdam, The Netherlands

[‖]Vrije Universiteit Amsterdam, De Boelelaan 1105, 1081 HV Amsterdam, The Netherlands.

Corresponding Authors

v.subramaniam@vu.nl

m.m.a.e.claessens@utwente.nl

[‡] These authors contributed equally to the work.

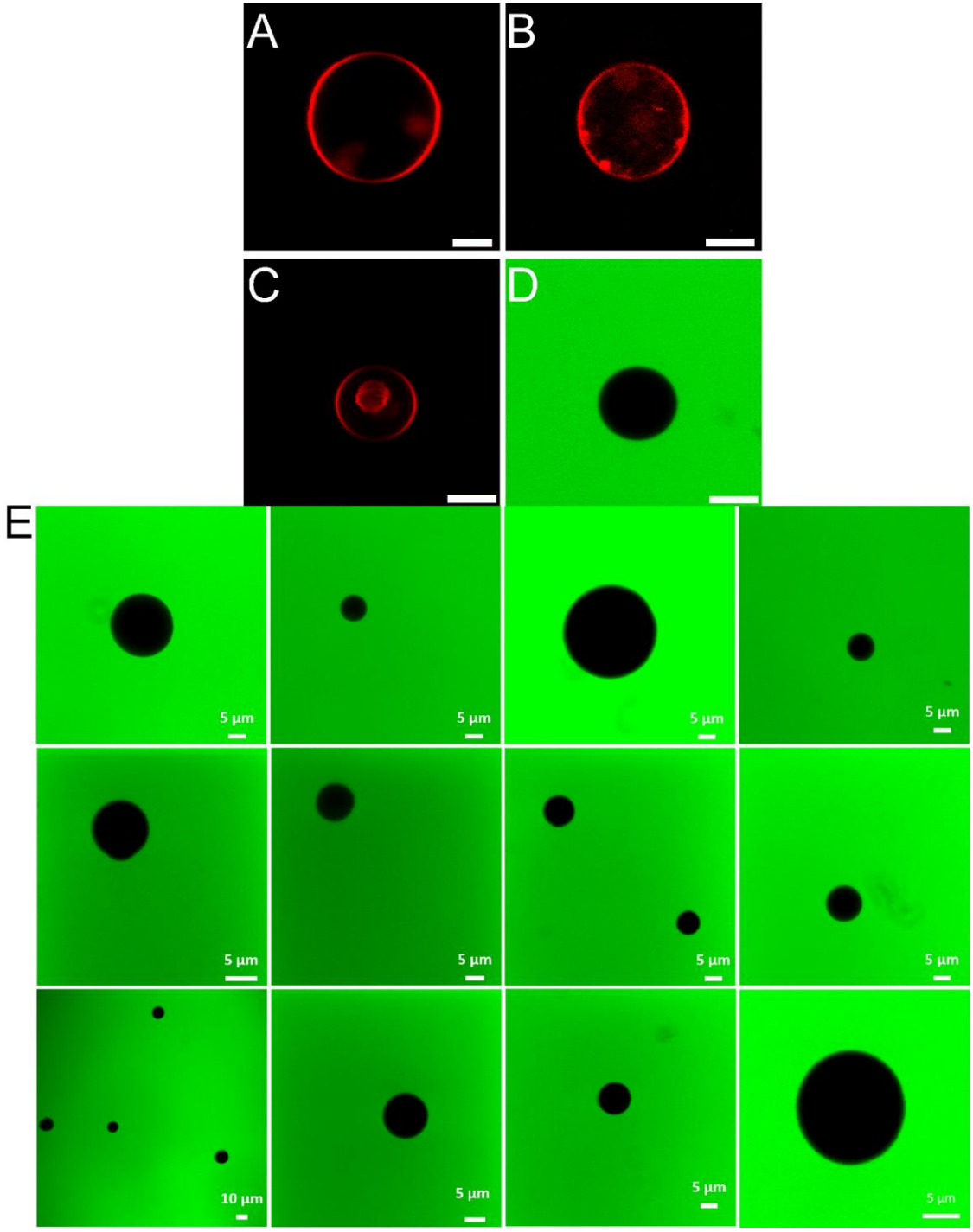

Figure S1: Representative images of immobilized POPC/POPS GUVs doped with Rh-DOPE (red) incubated with αS oligomers. POPC/POPS GUVs containing biotinylated lipids were immobilized on streptavidin-coated cover-slips. GUVs remain stable in the absence of αS oligomers (panel A) and even when incubated with 2.5 µM αS oligomers at room temperature for 20 hours (panel B). Scale bars are 5 µm in panel A and B. Panels C (red channel, GUV label) and D show images of GUVs incubated with 10 µM αS oligomer and calcein in the external solution at room temperature. Scale bars are 10 µm in panel C and D. Even after 24 hours of incubation with αS oligomers, vesicles remained intact and no influx of calcein was observed (Panel E).

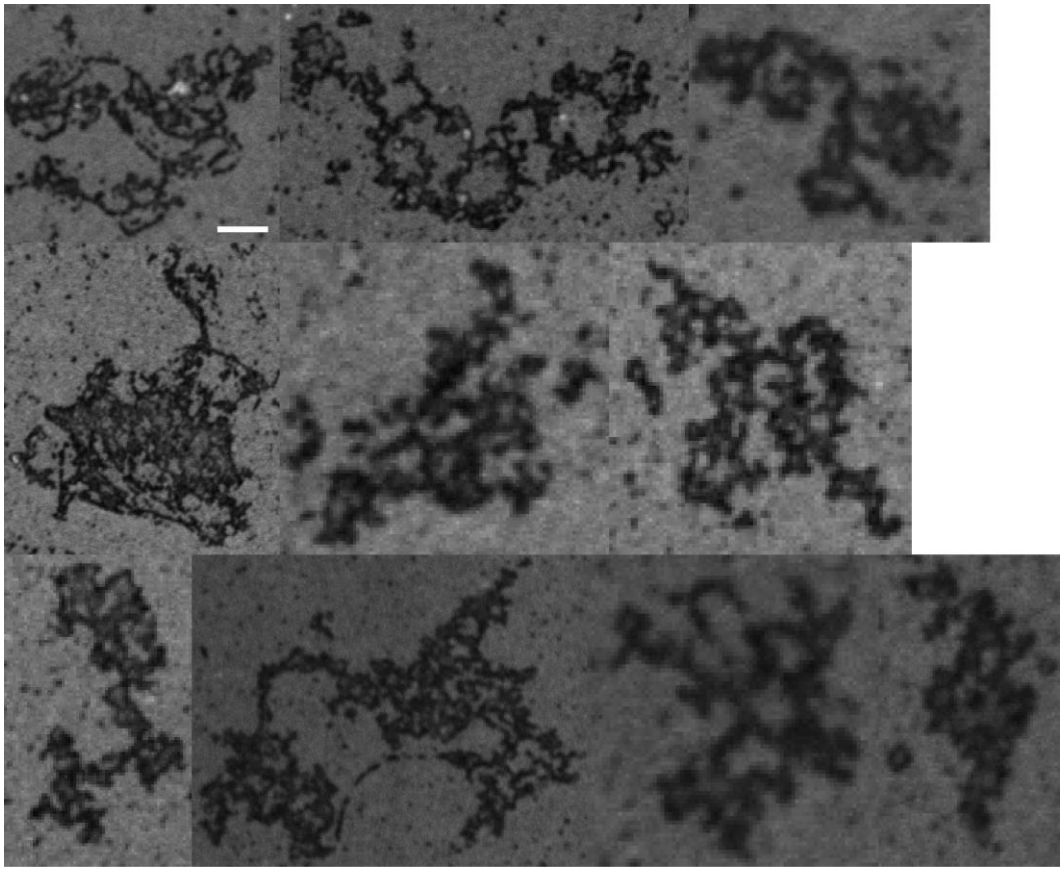

Figure S2: Analysis of αS oligomer induced membrane damage pattern by fluorescence confocal microscopy. (A) Representative gray-scale images showing damage patterns in Rhod-PE labeled POPC/POPS SLBs at room temperature acquired after 6 hours of incubation of 5 μM αS oligomers from two independent measurements. The SLBs were buffered with 10 mM Tris-Cl, 100 mM NaCl at pH 7.4. The scale bar is 2 μm.

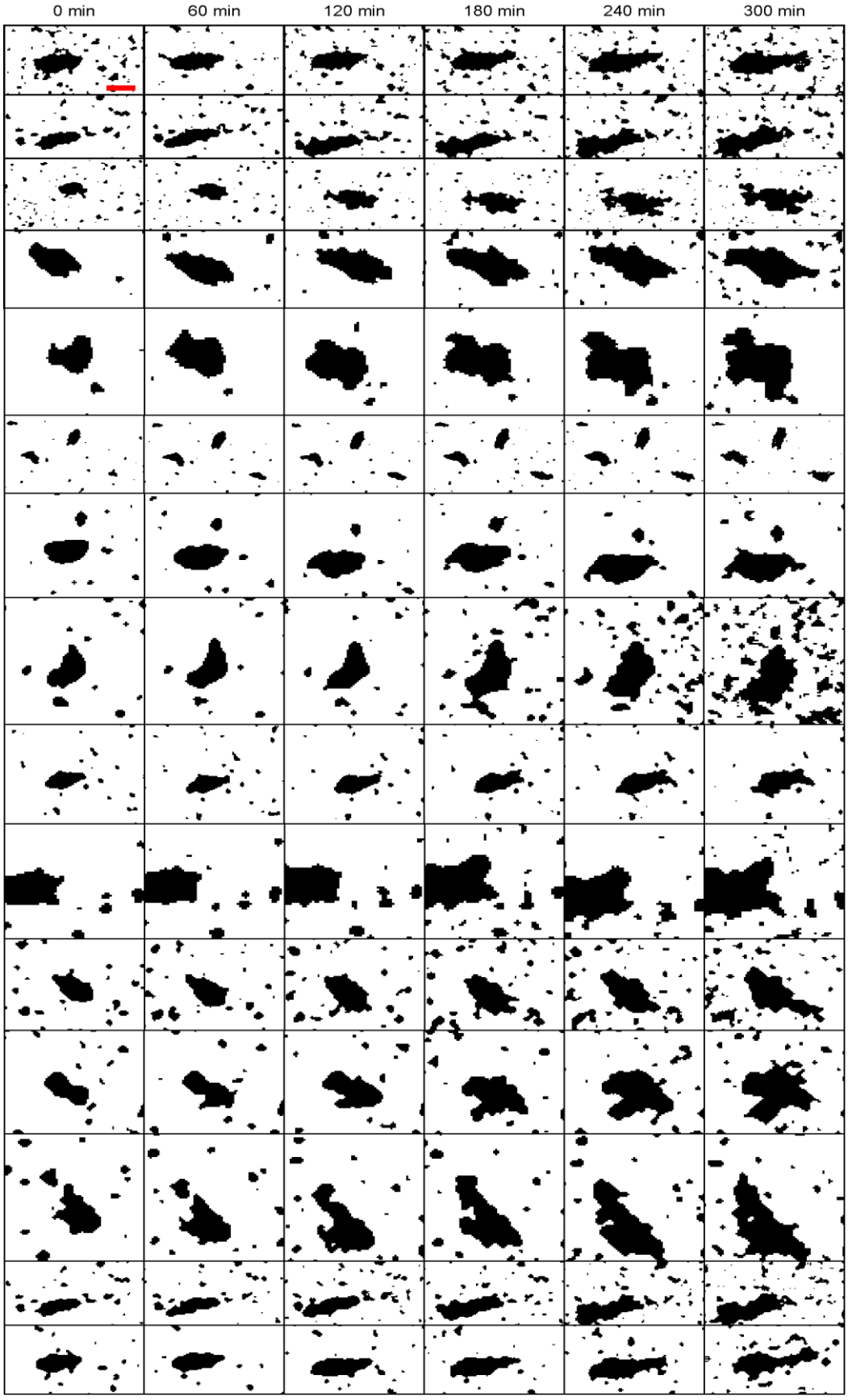

Figure S3: Time-lapse confocal images of evolution of damage patterns on POPC:POPS (1:1) SLBs on a PEG surface upon addition of αS oligomers. All time-lapse images from the lipid channel are converted to binary scale to aid visualization. The red scale bar is 2 μm.

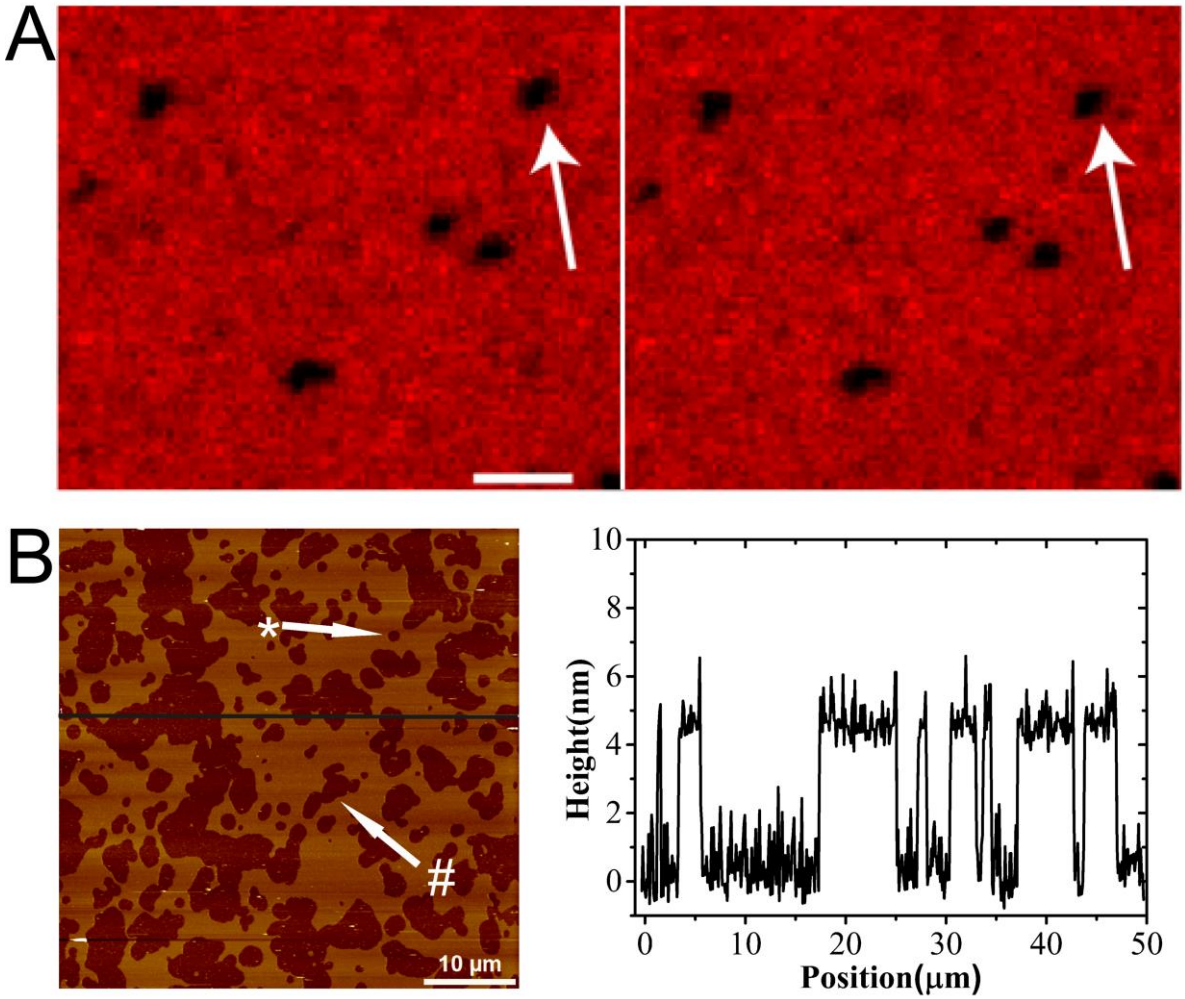

Figure S4: A) Confocal images of POPC:POPS (1:1) SLBs before (left) and after (right) WT-αS monomer addition. The panel on the right was acquired after 6 hours of incubation of 10 µM αS monomers and show slight decrease in defect areas (see white arrow). The quantification of the changes in defect area is shown in Figure 2A of the main text. The SLBs were buffered with 10 mM Tris-Cl, 100 mM NaCl at pH 7.4. The scale bar is 1 µm. B) AFM image of a defect containing POPC/POPS SLB in the absence of αS oligomers (left panel). Height profile of the SLB along the black line shown in right top panel. The height differences in the profile of ~5 nm correspond to the typical thickness of a lipid bilayer. White arrow indicates nearly circular defects (indicated by *) and several rounded defects merging (indicated by #).

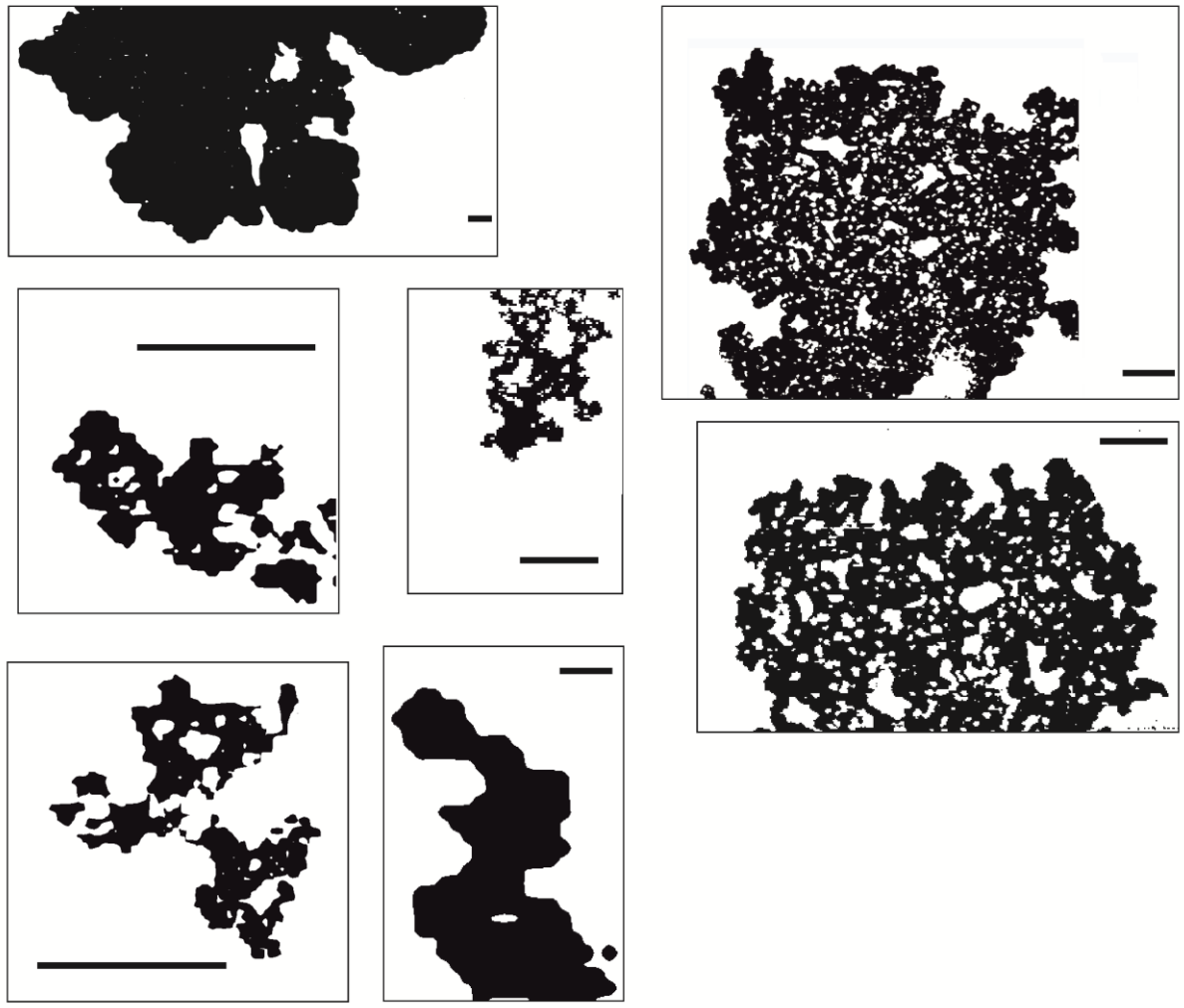

Figure S5: Overview of membrane damage patterns obtained from AFM images on POPC:POPS (1:1) SLBs on mica. All time-lapse images are converted to binary scale to aid visualization. The SLBs were buffered with 10 mM Tris-Cl, 100 mM NaCl at pH 7.4. Scale bar is 0.5 µm.

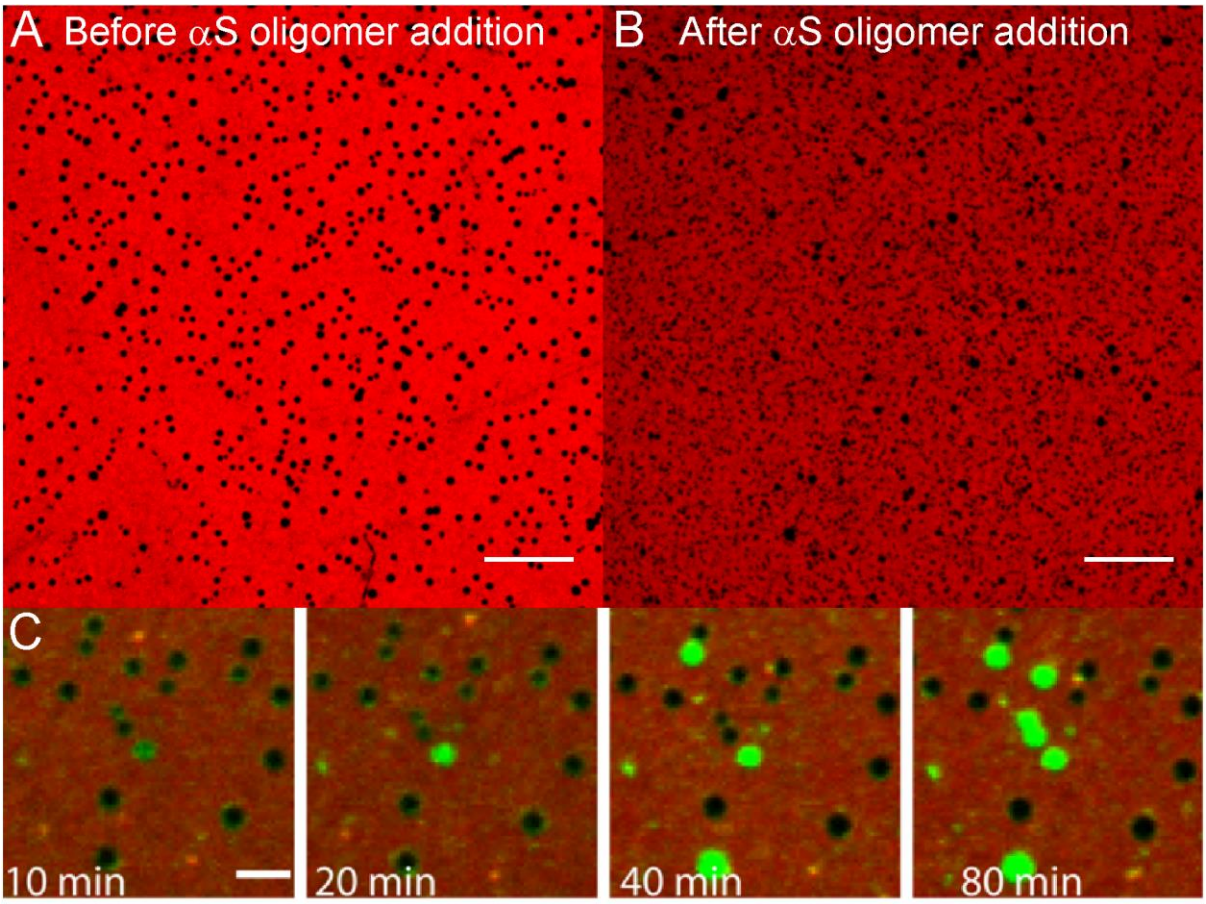

Figure S6: Rounded defects (panel A) in SLBs on glass substrate in absence of αS oligomers and irregularly shaped defects (panel B) in presence of αS oligomers. The scale bar is 10 μm. **C) αS oligomers accumulate at membrane defect edges.** POPC:POPS (1:1) SLBs were doped with 0.5 mol% Rhod-PE (red above). 5 μM of αS oligomers (10% AlexaFluor488 labeled, green above) was added to SLBs with preexisting defects. A green fluorescence ring is seen along the defect edges before it filles up αS oligomers from the solution. The SLBs were buffered with 10 mM Tris-Cl, 100 mM NaCl at pH 7.4. All measurements were conducted at room temperature. The scale bar is 2.5 μm.